Journal of Photochemistry and Photobiology A: Chemistry 217 (2011) 326–332

Contents lists available at ScienceDirect

Journal of Photochemistry and Photobiology A: Chemistry

journal homepage: www.elsevier.com/locate/jphotochem

The effect of Au on TiO_2 catalyzed selective photocatalytic oxidation of cyclohexane

Joana T. Carneiro [a], Tom J. Savenije [b], Jacob A. Moulijn [a], Guido Mul [c,*]

[a] Catalysis Engineering, ChemE, Delft University of Technology, Julianalaan 136, 2628 BL Delft, The Netherlands
[b] Opto-Electronic Materials, ChemE, Delft University of Technology, Julianalaan 136, 2628 BL, Delft, The Netherlands
[c] PhotoCatalytic Synthesis Group, Faculty of Science and Technology, University of Twente, Postbus 217, 7500 AE Enschede, The Netherlands

ARTICLE INFO

Article history:
Received 16 July 2010
Received in revised form
30 September 2010
Accepted 30 October 2010
Available online 5 November 2010

Keywords:
Au/TiO_2
Visible-light
Thermal effects
ATR-FTIR
Photocatalysis
TRMC

ABSTRACT

Gold does not induce visible light activity of anatase Hombikat UV100 in the selective photo-oxidation of cyclohexane, as can be concluded from in situ attenuated total reflectance Fourier transform infrared (ATR-FTIR) measurements. Extremely small conductance values measured at 530 nm in Time Resolved Microwave Conductivity (TRMC) experiments are in agreement with this conclusion. Upon UV activation, gold enhances the initial rate of formation of surface adsorbed cyclohexanone, but is detrimental to the overall production rate determined in a conventional top illuminated slurry reactor. The latter is the result of strongly modified surface properties of TiO_2 by gold deposition, affecting the adsorption/desorption equilibrium of cyclohexanone.

© 2010 Elsevier B.V. All rights reserved.

1. Introduction

Metal nanoparticles are of great interest because of their unique electronic, optical and magnetic properties. The spectroscopy of noble metal particles is associated with surface plasmon resonance, which is a collective oscillation of free conduction band electrons [1]. In particular, the strong plasmon absorbance of Au nanoparticles has attracted attention [2,3] for a wide variety of applications. Modification of TiO_2 photocatalysts with Au has also been extensively evaluated. Several authors observed visible light activity of Au/TiO_2 catalysts, tentatively explained by optical absorption of the Au nanoparticles [4–7]. In photocatalytic wastewater degradation, gold nanoparticles supported on TiO_2 have also been found to promote the activity upon UV excitation. This is generally explained by a catalytic effect of Au in transferring UV-photoexcited conduction band electrons of titania to the reacting substrate, typically O_2. The remaining free holes diffuse towards the titania surface and are able to oxidize surface adsorbed species [8–13]. Some of us have recently demonstrated, however, that this positive effect of Au deposition can be over-compensated by the detrimental loss of surface Ti-OH-groups during catalyst preparation, in particular if a deposition–precipitation method is used [14].

In the present work, we will first demonstrate that incipient wetness impregnation of metallic gold nanoparticles stabilized by poly(vinyl-pyrrolidone), leads to a smaller decrease in initial surface activity upon UV excitation of Hombikat TiO_2, as compared to catalysts prepared by precipitation. As will be shown by in situ ATR-FTIR measurements, Au also leads to enhanced adsorption of cyclohexanone. To the best of our knowledge, the potential of visible light activation of Au/TiO_2 to initiate cyclohexane oxidation has not been previously assessed, and will be demonstrated not to lead to the formation of cyclohexanone. Finally, the results will be discussed on the basis of Time Resolved Microwave Conductivity (TRMC) experiments.

2. Experimental

2.1. Catalyst preparation and characterization

Hombikat UV100 TiO_2 (Sachtleben GmbH), H, was used as received. It consists of 100% anatase as determined by XRD, and has a surface area of 337 $m^2\,g^{-1}$ with an average particle size of 7 nm [15]. This material was used to prepare a Au/TiO_2 photocatalyst, AuH, by an incipient wetness impregnation method, using a Au colloidal solution prepared as described by Lu et al. [16]. In short, metallic gold nanoparticles with poly(vinyl-pyrrolidone) (PVP) were prepared following a methodology, which involved the reduction of the metal salt by 120 mL anhydrous ethylene

* Corresponding author.
E-mail address: G.Mul@utwente.nl (G. Mul).

1010-6030/$ – see front matter © 2010 Elsevier B.V. All rights reserved.
doi:10.1016/j.jphotochem.2010.10.027

glycol (Sigma–Aldrich) in the presence of PVP (0.8 g, PVP40T, Sigma–Aldrich) at 353 K for 3 h. The obtained solution exhibited a deep red color. For impregnation of TiO_2, ~4 mL of the Au solution with a Au concentration of 2.6 mg mL^{-1} was used to impregnate 1 g of Hombikat. After the impregnation step the catalyst was dried in a static air oven at 120 °C overnight, and used without further calcination.

ICP analysis was performed to analyze the amount of Au present in the AuH catalyst, using a ICP-OES PerkinElmer Optima 3000dv instrument in the axial mode. The AAS instrument used was a PerkinElmer Analyst 100. About 25 mg of the sample was shaken well in a 25 mL mixture of 1% HF and 1.25% H_2SO_4 until complete dissolution, followed by analysis. A standard solution of Au (range 0–30 mg L^{-1}) was used for calibration.

Transmission electron microscopy (TEM) was performed on a Philips CM30UT electron microscope with a FEG (field emission gun) as the source of electrons operated at 300 kV. Samples were mounted on a copper supported Quantifoil microgrid carbon polymer.

UV/vis spectra of porous films of the catalysts, deposited by solvent (water) evaporation under vacuum onto a 1 mm thick quartz plate, were recorded on a Perkin-Elmer Lambda 900 spectrometer equipped with an integrating sphere (Labsphere).

Thermogravimetric analysis (TGA) of the catalysts was carried out on a TGA/SDTA851e thermobalance (Mettler-Toledo). The sample powders were heated from 298 to 1073 K at a heating rate of 10 K min^{-1}, in a flow of 100 mL min^{-1} of He or air, respectively.

2.2. Time Resolved Microwave Conductivity experiments

For the Time Resolved Microwave Conductivity (TRMC) measurements, a porous film of the catalysts was deposited by solvent (water) evaporation onto a 1 mm thick quartz plate. The TRMC technique is based on the measurement of the normalized change of microwave power reflected by a sample after illumination by a laser pulse at a variable wavelength. In this work two wavelengths were chosen: 300 nm (UV-light) and 530 nm (visible light). The intensity of the laser pulse was varied using a set of metallic neutral density filters. The normalized change in microwave power reflected by the sample, $\Delta P(t)/P$, is caused by a change of the conductance induced by the laser pulse, $\Delta G(t)$, which correlates with the product of the charge carrier formation and the sum of electron and hole mobilities, $\eta\Sigma\mu_i$. A full description of the microwave circuit and the data analysis is given elsewhere [17]. The time-resolved microwave signal obtained on excitation with a nanosecond laser pulse, can be characterized by two stages. Up to approximately 30 ns, the signal is dictated by the instrumental response time. After this initial stage, the signal decays due to trapping or recombination of charge carriers. As the signal decay is not exponential, the general decay shape is characterized by the halftime, $\tau_{1/2}$, defined as the period involved to reduce to half of its maximum value. Due to their higher mobility, electrons contribute far more to the photoconductance in TiO_2 nanoparticles [17] than positive charges and, therefore $\sum\mu_i$ is assumed to be close to the electron mobility, $\mu_e^{\sim}$.

2.3. Photo-activity measurements

To evaluate catalyst performance in the selective oxidation of cyclohexane upon UV illumination, reactions were carried out in a top illumination reactor (TIR), as described previously [14]. In a typical experiment 100 mL of cyclohexane containing 1 g L^{-1} of catalyst was used (slurry system). The catalysts were dried for 1 h at 120 °C to remove adsorbed water and impurities, prior to suspension. The solution was illuminated from the top of the reactor through a Pyrex window that cuts off the highly energetic UV radiation [18]. A high pressure mercury lamp of 50 W was used (HBO50W from ZEISS). The light intensity of the lamp used in the wavelength absorption range of TiO_2 (275–388 nm) is 2×10^{-7} Einst cm^{-2} s^{-1}, determined at the position of the Pyrex window, *i.e.* where light is entering the reactor. Air dried over Molsieve 3 Å, (Acros Organics) and presaturated with cyclohexane, was bubbled through the TiO_2 suspension at a rate of 30 mL min^{-1}. During the reaction liquid was withdrawn in aliquots of 0.2 mL and analyzed by GC. Organic compounds were quantitatively analyzed twice using a flame ionization detector and a Chrompack, CPwax52CB column. Hexadecane was used as an internal standard. After reaction in the top illumination reactor, the catalyst was filtered and TGA was performed in order to determine the nature of surface adsorbed species.

The performance of the materials was also evaluated using our home-built ATR-FTIR operando system and the procedure is described in detail elsewhere [19]. Two different LED sets were used with different wavelengths: 375 nm with 9×10^{-9} Einst cm^{-2} s^{-1} intensity, and 530 nm with 3×10^{-8} Einst cm^{-2} s^{-1} intensity. The catalysts were coated on a ZnSe ATR crystal yielding an approximate 1.0 μm thick coating. Oxygen saturated cyclohexane was flown at 8.75 mL min^{-1} through the ATR cell. Prior to photocatalytic oxidation experiments, adsorption of cyclohexane on the TiO_2 was monitored for 90 min and a spectrum of adsorbed cyclohexane on TiO_2 was used as background for the photo-oxidation experiments. The background and the sample spectra were averaged from 64 and 32 spectra, respectively. Both reactor systems were equipped with a cooling system to keep the reaction temperature at 25 °C and to avoid cyclohexane evaporation.

3. Results

3.1. Characterization

Fig. 1a shows the UV/vis spectra of both materials under investigation. The absorbance, F_A, is the relative amount of photons actually attenuated by the catalyst layer, defined as

$$F_A = \frac{I_0 - I_T - I_R}{I_0}$$

where I_0, I_T and I_R are the incident, transmitted and reflected light intensities, respectively. For the purple material AuH, the UV/vis spectrum shows a broad absorbance with a maximum at ~530 nm, which is assigned to the plasmon resonance absorption of metallic Au nanoparticles. This optical transition is the result of collective oscillations of electrons at the nano-particle surface at a specific frequency [20]. This transition appears as a broad band in the optical absorbance spectrum due to the thickness of the AuH sample which is of several microns.

The particle size distribution of the Au nanoparticles deposited on the TiO_2 is depicted in Fig. 1b. The distribution shows that most of the Au particles are <4 nm. The largest particles are ~16 nm. A TEM micrograph revealing ~6 nm Au particles on the TiO_2 surface is shown in the inset. The image also shows that H consists of nanocrystallites inter-connected to form a three-dimensional porous network, and that this TiO_2 sample does not consist of well defined separated crystals, as discussed previously [21]. The Au loading was determined to be 0.8 wt.% by ICP analysis.

3.2. Activity determination in the top illumination reactor

Previous work showed that the main products of photocatalytic cyclohexane oxidation are cyclohexanone and cyclohexanol, with a ketone over alcohol selectivity higher than 98% [14,15,22]. Cyclohexane conversion is below 2%, and CO_2 contributions, due to complete oxidation, are not significant (cyclohexanone and cyclohexanol are reported to be produced with selectivities >95% relative to CO_2) [15]. While radical chemistry in solution can lead to other

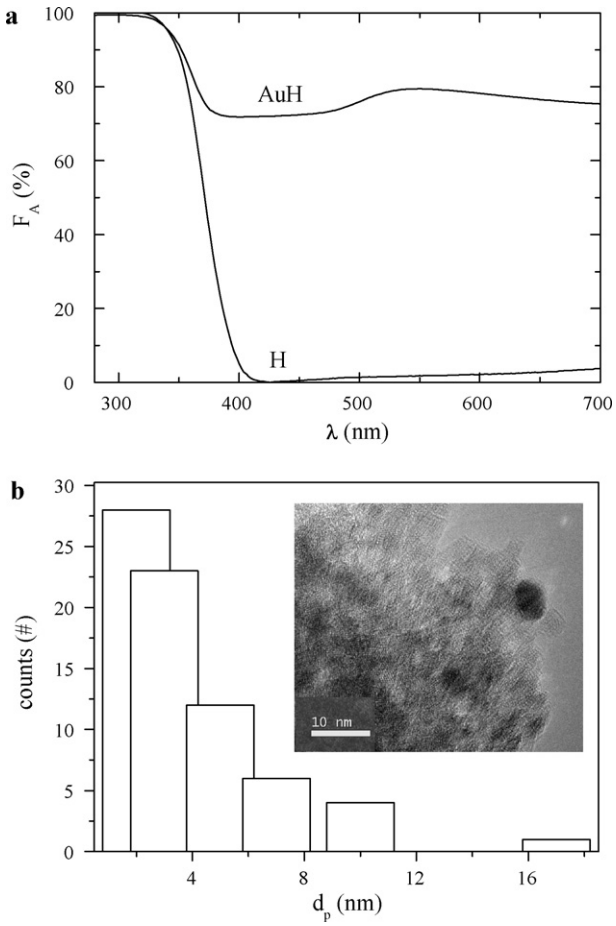

Fig. 1. (a) UV/vis attenuation spectra of the studied materials in terms of absorbed fraction (F_A). (b) Particle size distribution of the Au nanoparticles deposited on TiO_2, AuH. The inset shows a TEM micrograph of the AuH material with an Au nanoparticle of ~6 nm in size.

products, in view of the applied wavelengths (>275 nm) this is not expected to occur, as is confirmed by our GC analyses.

Cyclohexanone formation upon photo-oxidation of cyclohexane is shown in Fig. 2e for the two catalysts. The shape of the profiles, *i.e.* the presence of a plateau, is the result of catalyst deactivation, induced by carbonate and carboxylate formation on the catalyst surface [19]. The amount of cyclohexanone formed as well as its initial reaction rate is slightly higher for the H material when compared to AuH. In addition to cyclohexanone production, the inset shows the cyclohexanone/cyclohexanol selectivity defined as $n_{cyclohexanone}/(n_{cyclohexanol} + n_{cyclohexanone}) \times 100$ during the reaction

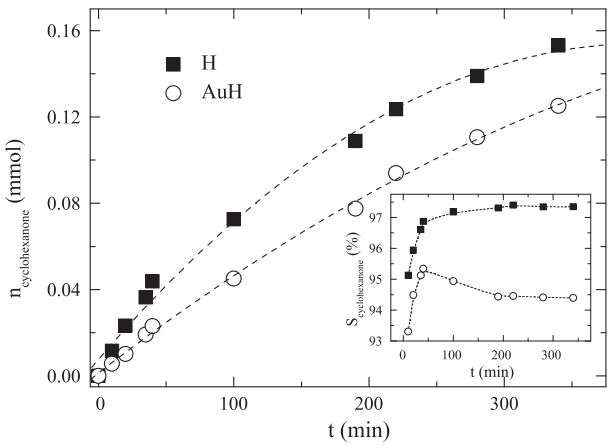

Fig. 2. Cyclohexanone production profiles in the TIR for H and AuH. The cyclohexanone value reaches a plateau after prolonged time of reaction, as a result of loss of activity of the catalyst. The inset shows the cyclohexanone/cyclohexanol selectivity during reaction for the two materials.

period for both materials under investigation. The AuH material showed an increase in cyclohexanol selectivity [9,14].

In Fig. 3a, a set of TGA profiles is shown for the samples before (fresh) and after (spent) the photocatalytic reaction performed in the TIR, expressed as the derivative in time of the weight loss of the materials at a given reference temperature. In the profiles, two peaks at 60 °C and 240 °C are present, which are in agreement with previously reported data [21]. The first desorption peak at 60 °C corresponds to adsorbed water, which after reaction is less for all the samples. Surprisingly, the weight loss at 240 °C is considerably higher for the spent AuH catalyst, Fig. 3b, as compared to the spent H sample, Fig. 3a. Because this peak is accompanied by an exothermic effect, this is assigned to (hydro)carbon containing adsorbates formed during reaction. The total weight loss increases in the following order: $H_{spent} < Au_{Hspent} < AuH < H$.

3.3. Time Resolved Microwave Conductivity

Fig. 4 shows the TRMC transients obtained upon excitation of the samples at 300 nm and 530 nm wavelength at laser pulse intensities of 24 μJ cm^{-2} and of ~0.1 mJ cm^{-2}, respectively. A high laser intensity was used, because of the small signal obtained for the samples at 530 nm at lower intensities. The maximum incident-intensity normalized photo-conductance of the different samples follows the order H (300 nm) > AuH (300 nm) > H (530 nm) > AuH (530 nm). In the case of 530 nm excitation, the AuH and H catalysts show a positive region until 30 ns, after which for AuH a negative conductance value (imaginary conductance) is

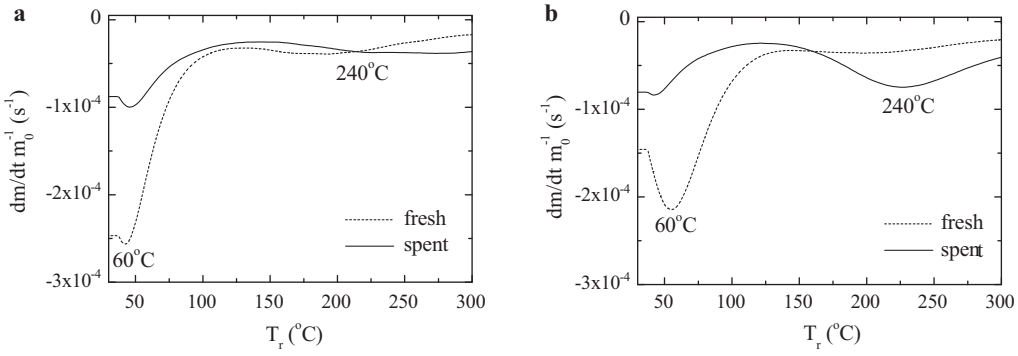

Fig. 3. TGA profiles under a He flow as weight loss vs reference temperature of the fresh and spent materials collected after reaction in the TIR and of the fresh catalysts for (a) H and (b) AuH.

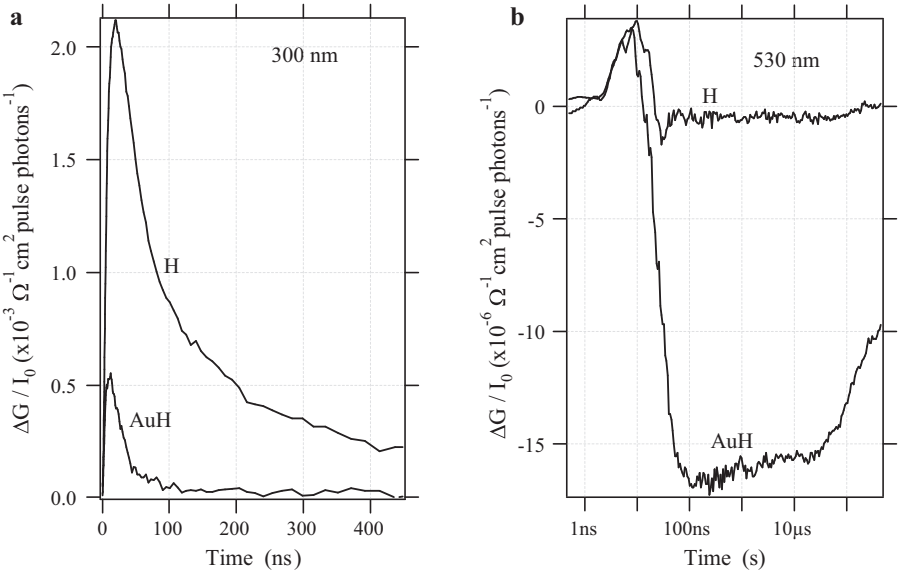

Fig. 4. Incident intensity-normalized conductance ($\Delta G/I_0$) transients obtained for the samples, H and AuH, studied at (a) 300 nm and (b) 530 nm laser wavelength (note the different *Y* axis scale). It should be taken into account that for the AuH transients at 530 nm, the typically used equations for conductance calculation [9] are no longer valid, in view of the negative values.

observed at longer lifetimes. For H the conductance approaches zero.

3.4. ATR-FTIR

In the in situ ATR-FTIR spectra of the reaction performed under 375 nm irradiation, two regions are of interest [19]. The high wavenumber region, where stretching vibrations of OH-groups (3637 cm^{-1}) and adsorbed water are to be expected (3350–3380 cm^{-1}), and the low wavenumber region, where cyclohexanone bands (1689 cm^{-1} and 1714 cm^{-1}), carboxylate (taken between 1589 and 1544 cm^{-1}, [23,24]), and carbonate bands (1403 cm^{-1}, [24,25]) appear. The spectral development during reaction in the low wavenumber region is shown in Fig. 5, for both materials under study. It is apparent that in the early stages of reaction a broad range of infrared absorptions develops between 1800 and 1000 cm^{-1}. The C=O stretching mode assigned to bulk cyclohexanone can be followed by the band at 1714 cm^{-1}, and the one corresponding to the adsorbed analogue by the band at 1690 cm^{-1} [19]. The development of the spectra of H, Fig. 5a, shows qualitatively the same bands as AuH, Fig. 5b, but the intensities are different, especially in the area where the peaks of adsorbed and bulk cyclohexanone are present. A persisting higher intensity of the 1690 cm^{-1} band in the case of AuH is observed.

In Fig. 6 the peak height evolution during photocatalytic oxidation of cyclohexane with 375 nm irradiation for two absorptions assigned to the OH-groups sites, 3633 cm^{-1}, referred to as $(Ti)_2$-OH, and the OH stretching vibration of adsorbed water molecules centred at 3375 cm^{-1} is shown. Generally, in the beginning of the reaction the water amount at the catalyst surface increases and after ~20 min starts to decrease, eventually becoming negative until a minimum plateau is reached. The water amount formed dur-

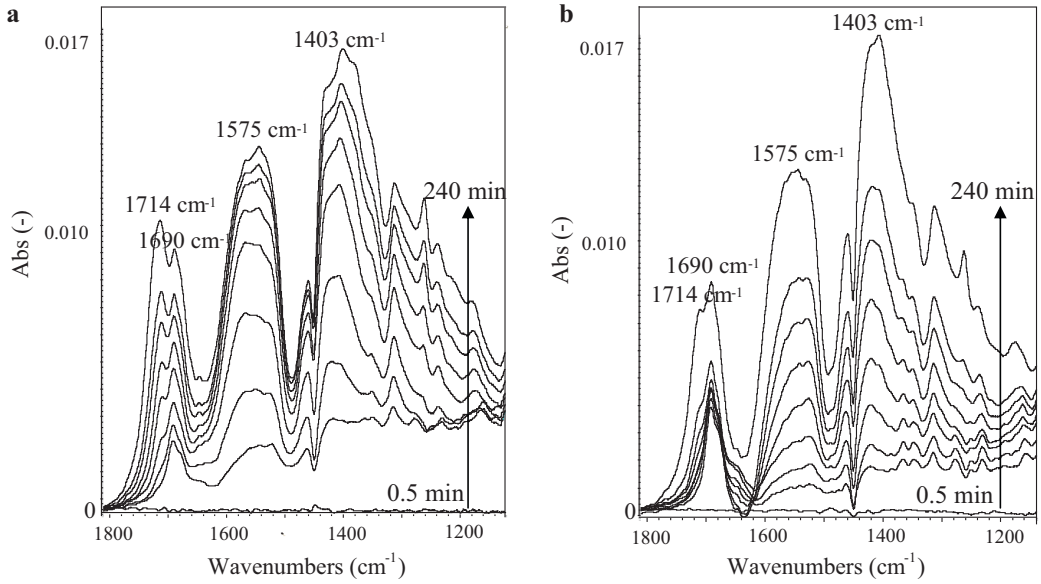

Fig. 5. ATR-FTIR spectra of cyclohexane photocatalytic oxidation on (a) H and (b) AuH coated on a ZnSe crystal with light irradiation wavelength of 375 nm. The spectra were recorded between 0.5 and 240 min of reaction time. The wavenumbers of the most important bands, representing product formation at the catalyst surface, are depicted.

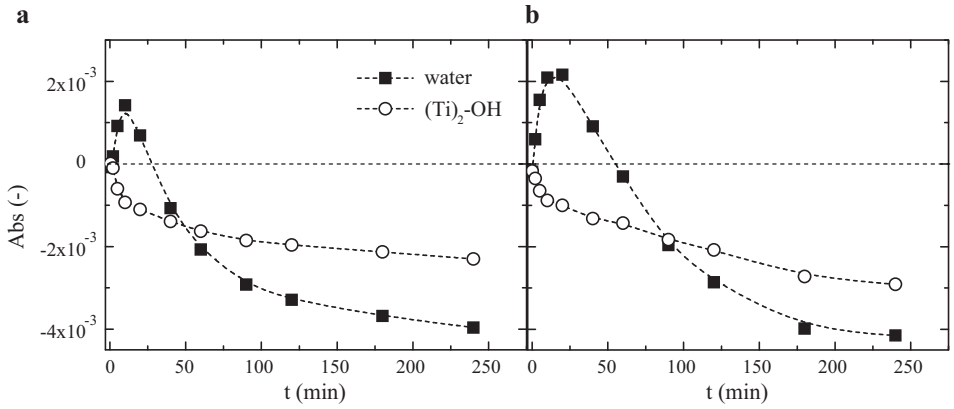

Fig. 6. Time evolution of the selected peaks, adsorbed water centred at 3375 cm^{-1} and bridged $(Ti)_2$-OH group at 3633 cm^{-1}, from the spectra measured with the ATR-FTIR system for (a) H and (b) AuH with light irradiation at 375 nm.

ing reaction is higher in the case of the AuH material and also the OH-groups decrease (are covered) more significantly for the AuH sample as compared to H.

Using deconvolution of the peaks assigned to bulk and desorbed cyclohexanone [21], the time profiles shown in Fig. 7 were obtained. For both materials the time profiles show that in the first 10 min of reaction the amount of adsorbed cyclohexanone increases at a high rate followed by a slower increase. Bulk cyclohexanone also increases, but at a slower rate. The initial rate of adsorbed cyclohexanone is faster for the AuH catalyst, Fig. 7b, compared to H, Fig. 7a. In the case of AuH there is a well defined plateau of adsorbed cyclohexanone between 20 and 120 min followed by a continuous increase. In the case of AuH the bulk cyclohexanone formation rate increases after ~120 min of reaction. The H profiles show that the adsorbed cyclohexanone reaches a plateau after 100 min of reaction, while the bulk cyclohexanone amount increases continuously.

Fig. 8 shows the spectral evolution during reaction time under 530 nm light irradiation. None of the bands correspond to species formed when the reaction is performed under UV-light irradiation. Considering the very low absorption intensities, we can state that cyclohexane selective oxidation is not taking place at 530 nm light irradiation for both materials. The bands present at 1124 and 1162 cm^{-1} (left shoulder in the previous peak) can be assigned to cyclohexane adsorption. The bands at 1450 cm^{-1} and 1260 cm^{-1} are characteristic of the scissoring and twisting vibrations, respectively, of CH_2 groups in cyclohexane [19]. These bands are increasing in both materials except for the absorption at 1450 cm^{-1} for AuH, Fig. 8b, which is decreasing. The decreasing band at 1640 cm^{-1} corresponds to the removal of water from the surface, already present in the catalyst layer at the beginning of the reaction.

4. Discussion

4.1. UV-photocatalysis

First it is important to note that as a result of Au deposition on Hombikat UV100, the amount of surface bound water and OH groups decreases (Fig. 3), diminishing the initial reaction rate of production of cyclohexanone, Fig. 2. The negative effect of Au deposition observed in Fig. 3, is not as extensive as previously reported [14]. The explanation is based on the different synthesis methods: the impregnation method to deposit Au nanoparticles on the TiO_2 surface used in this work apparently did not induce as much surface modifications as the deposition–precipitation method used previously [14].

The cyclohexanone/cyclohexanol selectivity of the AuH catalyst is lower than obtained with H. This is expected, since upon UV-light activation the electrons in the conduction band of TiO_2 are transferred to the Au nanoparticles [9], and the induced charge separation will increase the concentration of OH-radicals at the TiO_2 surface, consecutively generating a higher transient concentration of cyclohexyl hydroperoxide radicals. This increases the probability of the reaction of two cyclohexyl hydroperoxide radicals to yield cyclohexanol [14,22]. Since the preparation procedure of AuH was different as compared to reported in Ref. [9], new TRMC measurements at 300 nm were performed, Fig. 4a, and as expected, the conductance signals obtained lead to the same conclusions reported previously [9]. The photoconductance values and electron lifetimes in TiO_2 are lower under UV-light excitation when Au is present, due to the fact that upon formation of an electron–hole pair, electrons will migrate to the Au nanoparticles. Ti-OH sites around the perimeter of Au particles have been previously iden-

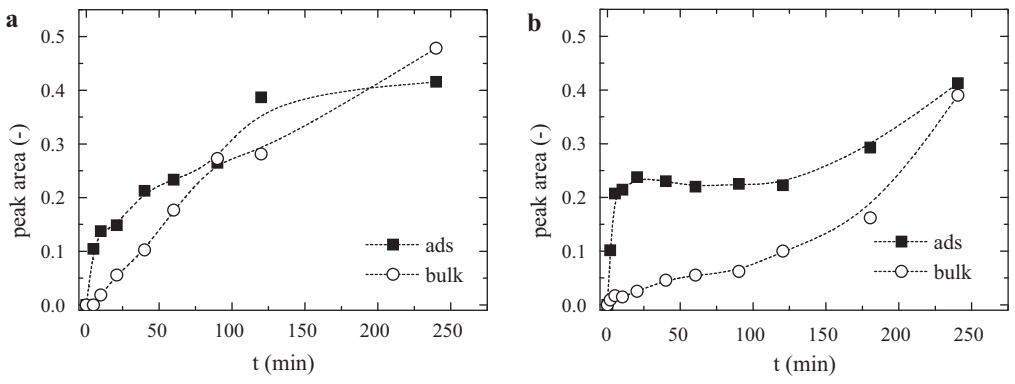

Fig. 7. Bulk and adsorbed cyclohexanone time profiles obtained from peak deconvolution until 240 min of reaction for (a) H and (b) AuH with light irradiation wavelength of 375 nm.

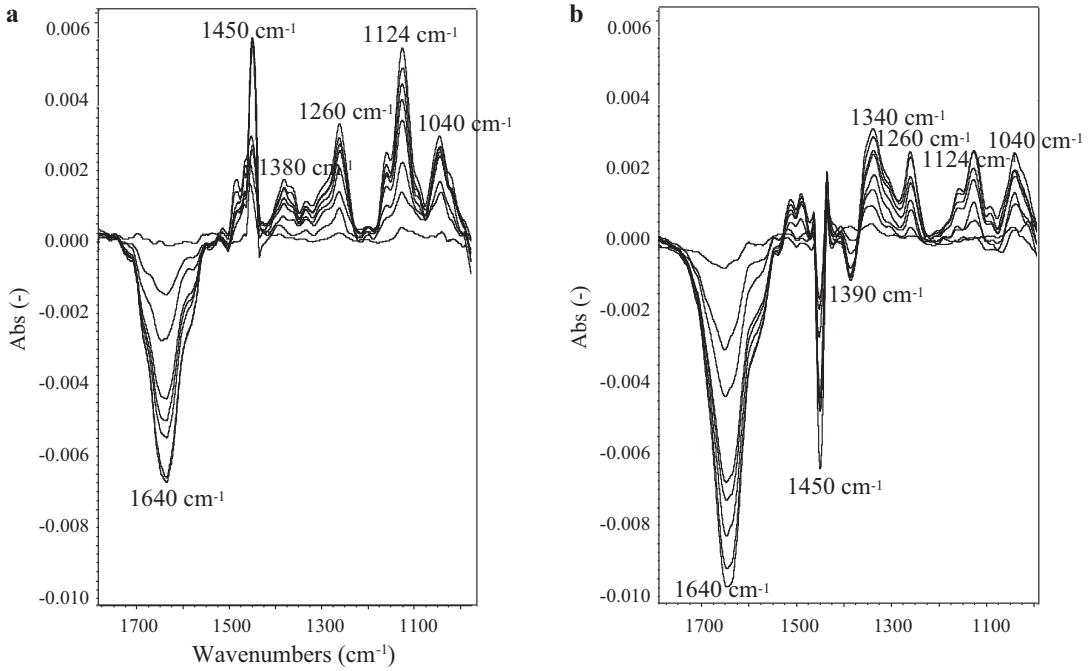

Fig. 8. ATR-FTIR spectra of cyclohexane photocatalytic oxidation on (a) H and (b) AuH coated on a ZnSe crystal with light irradiation wavelength of 530 nm. The spectra were recorded between 0.5 and 90 min of reaction time. The wavenumbers of the most important peaks are depicted.

tified as more reactive in 'thermal' applications of Au/TiO_2. We believe these sites are also very effective in photocatalysis, since these are the most likely to be benefiting from the presence of Au in making charge separation more efficient.

According to a previously proposed reaction mechanism, surface adsorbed water is formed upon formation of a cyclohexyl radical (*i.e.* OH-radical oxidation of cyclohexane), Eq. (1) [22]. The profiles shown in Fig. 7 reveal that more water is formed in the case of the AuH material. Furthermore, the higher water content is also reflected by the decreasing intensity of the $(Ti)_2$-OH sites, which is more significant for AuH than for H.

$$C_6H_{12}+OH^{\bullet} \rightarrow C_6H_{11}^{\bullet}+H_2O \quad (1)$$

The fact that water is formed in higher amounts over the AuH material suggests a higher rate of formation of surface adsorbed cyclohexanone, which is in agreement with the data shown in Fig. 7 for the first ~25 min of reaction.

The trends shown in Fig. 7, can be explained by a two site adsorption model discussed in previous work, where one site gives strong adsorption, in the early stages of the reaction, and the other weaker adsorption at later stages of the reaction [21]. Fig. 7b suggests that this model is also valid for the AuH material, demonstrating that the first *plateau* of adsorption is even clearer than for H. This might be related to the sites in close proximity of the Au particles, which are proposed to be more reactive than 'remote' sites. The final absorption values for adsorbed cyclohexanone are comparable. This is expected, since the number of OH-groups involved is practically the same. It should be noted that the presence of Au seems to enhance the reactivity of the most active sites of TiO_2, yielding predominantly adsorbed cyclohexanone. This is confirmed by the thermogravimetrical results presented in Fig. 4 where the peak at 240 °C increased more significantly for AuH as compared to H. Although the existence of two types of sites for cyclohexanone adsorption is in agreement with the model reported previously for this reaction, the chemical nature of the sites is yet unknown.

The ATR-FTIR results shown in Fig. 5 are inconclusive with respect to cyclohexanol formation. Although this compound is detected in the TIR, in the ATR-FTIR analysis the complexity of the overlapping bands in the spectral range where absorptions of cyclohexanol are expected, renders identification difficult. This region is composed of a multitude of absorptions assigned to various carbonate and carboxylate species [19,22]. Furthermore, and according to the light intensities used in both reactors, which is considerably higher in the TIR experiment, the yields are likely too small to be detected.

4.2. Visible-light photocatalysis

Based on observations in femtosecond transient absorption spectroscopy involving a visible excitation pulse in combination with an IR probe, Furube et al. observed plasmon induced electron transfer from 10 nm Au nanoparticles to TiO_2 [26]. These plasmon electrons in the conduction band of TiO_2 are claimed to reduce molecular oxygen at the TiO_2 surface efficiently, while the remaining electron deficit in the Au nanoparticles should be able to oxidize organic compounds [4]. This model has been used to explain the photocatalytic activity of Au/TiO_2 in methylene blue degradation upon visible light activation [5]. If the steps indicated above would be effective, 530 nm laser activation of Au/TiO_2 should result in electron mobility in TiO_2. The photo-conductance values presented in Fig. 5 show that in Hombikat with and without Au promotion electron mobility is in fact very small: ~1000 times lower at 530 nm as compared to activation at 300 nm. The thus apparent absence of electron transfer from Au to TiO_2 is in line with previous studies using time resolved optical measurements to analyze photo-activation of gold nano-particles, which report sub-nanosecond recombination of plasmon excited states [26]. The TRMC equipment used for our study is limited to the nanosecond timescale, so this recombination process is not observed.

The striking negative feature (>30 ns) observed for AuH upon visible light excitation is also important to discuss. Due to the high visible light laser intensities, some Au nanoparticles might be melting under laser pulse excitation, as can be concluded from the following. Considering the value of the heat capacity for Au ($0.126\,J\,g^{-1}\,K^{-1}$), a particle diameter of 2 nm, and the energy of the laser pulse, $0.1\,mJ\,cm^{-2}$, the temperature rise, ΔT, within the Au

nanoparticle would be ~600 K. This means that the actual temperature in the Au nanoparticle is ~900 K. According to the melting point of Au particles with sizes below ~2.5 nm diameter which is reported to be below 700 K [27], the Au is in the liquid state at 300 K upon illumination. The melting phenomena of the Au nanoparticles explain the negative conductance values observed. This is due to the change of the real dielectric constant value of the sample, resulting in a shift of the resonance frequency of the loaded cavity, and the negative signal intensities [28]. In conclusion, reporting photon fluxes in studies on Au promoted photocatalysis is very important, to exclude contributions of thermo-catalysis.

In view of the above evaluation, a plasmon absorption induced electron transfer from Au to TiO_2 is not expected. Indeed, Fig. 8 does not provide evidence for the formation of cyclohexanone. Only a minor decrease in the amount of adsorbed water is observed, possibly related to the above mentioned heat effects. The positive spectral contributions in Fig. 8 are assigned to adsorbed cyclohexane exchanging with initially present surface adsorbed water. Since the time-scale for electron–hole recombination from the Au nanoparticles to the TiO_2 under visible light radiation is in the fs range, promoting TiO_2 with Au does not have a significant influence on the surface photo-chemistry, since the important time-scale for photocatalytic processes is usually in the μs time range.

5. Conclusions

Upon UV-light activation, the effective separation of electron–hole pairs induced by Au nanoparticles results in an enhanced concentration of hydroxyl radicals on the TiO_2 surface, and thus a higher initial rate of surface cyclohexanone formation. In addition, Au was found to decrease the desorption rate of cyclohexanone, which leads to lower production of cyclohexanone dissolved in cyclohexane, as analyzed using a top illumination reactor. Visible light activation of Au/TiO_2 photocatalysts does not initiate the studied reaction, in agreement with the absence of evidence for electron injection from Au into the conduction band of TiO_2. The TRMC data suggest the temperature of the Au particles might increase significantly upon light activation. We propose that visible light induced photocatalysis of Au promoted TiO_2 reported in the literature might be the consequence of these thermal effects, rather than the previously proposed electronic effects. The lifetime of the plasmon photon excited state is likely too short to initiate such effects.

References

[1] U. Kreibig, M. Vollmer, Optical Properties of Metal Clusters, Springer-Verlag, Berlin (1995).
[2] S. Link, M.A. El Sayed, J. Phys. Chem. B 103 (1999) 8410–8426.
[3] J.J. Mock, M. Barbic, D.R. Smith, D.A. Schultz, S. Schultz, J. Chem. Phys. 116 (2002) 6755–6759.
[4] E. Kowalska, R. Abe, B. Ohtani, Chem. Commun. (2009) 241–243.
[5] X.Z. Li, F.B. Li, Environ. Sci. Technol. 35 (2001) 2381–2387.
[6] R.S. Sonawane, M.K. Dongare, J. Mol. Catal. A: Chem. 243 (2006) 68–76.
[7] V. Rodriguez-Gonzalez, R. Zanellac, G. del Angela, R. Gomeza, J. Mol. Catal. A: Chem. 281 (2008) 93–98.
[8] H.X. Li, Z.F. Bian, J. Zhu, Y.N. Huo, H. Li, Y.F. Lu, J. Am. Chem. Soc. 129 (2007) 4538–4539.
[9] J.T. Carneiro, T.J. Savenije, G. Mul, Phys. Chem. Chem. Phys. 11 (2009) 2708–2714.
[10] S.C. Chan, M.A. Barteau, Langmuir 21 (2005) 5588–5595.
[11] A. Orlov, D.A. Jefferson, N. Macleod, R.M. Lambert, Catal. Lett. 92 (2004) 41–47.
[12] S. Sakthivel, M.V. Shankar, M. Palanichamy, B. Arabindoo, D.W. Bahnemann, V. Murugesan, Water Res. 38 (2004) 3001–3008.
[13] T. Sreethawong, S. Yoshikawa, Catal. Commun. 6 (2005) 661–668.
[14] J.T. Carneiro, C.C. Yang, J.A. Moma, J.A. Moulijn, G. Mul, Catal. Lett. 129 (2009) 12–19.
[15] P. Du, J.A. Moulijn, G. Mul, J. Catal. 238 (2006) 342–352.
[16] P. Lu, T. Teranishi, K. Asakura, M. Miyake, N. Toshima, J. Phys. Chem. B 103 (1999) 9673–9682.
[17] J.E. Kroeze, T.J. Savenije, J.M. Warman, J. Am. Chem. Soc. 126 (2004) 7608–7618.
[18] P. Du, J.T. Cameiro, J.A. Moulijn, G. Mul, Catal. Appl. A 334 (2008) 119–128.
[19] A.R. Almeida, J.A. Moulijn, G. Mul, J. Phys. Chem. C 112 (2008) 1552–1561.
[20] Y. Tian, T. Tatsuma, J. Am. Chem. Soc. 127 (2005) 7632–7637.
[21] J.T. Carneiro, J.A. Moulijn, G. Mul, J. Catal. 273 (2010) 199–210.
[22] J.T. Carneiro, A.R. Almeida, J.A. Moulijn, G. Mul, Phys. Chem. Chem. Phys. 12 (2010) 2744–2750.
[23] P.Z. Araujo, C.B. Mendive, L.A.G. Rodenas, P.J. Morando, A.E. Regazzoni, M.A. Blesa, D. Bahnemann, Colloids Surf. A 265 (2005) 73–80.
[24] D.J. Yates, J. Phys. Chem. 65 (1961) 746–753.
[25] P.A. Connor, K.D. Dobson, A.J. McQuillan, Langmuir 15 (1999) 2402–2408.
[26] A. Furube, L. Du, K. Hara, R. Katoh, M. Tachiya, J. Am. Chem. Soc. 129 (2007) 14852–14853.
[27] P. Buffat, J.P. Borel, Phys. Rev. A 13 (1976) 2287–2298.
[28] M.P. Dehaas, J.M. Warman, Chem. Phys. 73 (1982) 35–53.